

Squeezing and Entanglement Dynamics in Phase-Sensitive Non-Hermitian Systems

Ruicong Huang,^{1, 2, 3, *} Wencong Wang,^{3, 4, *} Yuyang Liang,^{1, 2, 3} Dongmei Liu,^{3, 4, †} and Min Gu^{1, 2, 3, ‡}

¹*Key Laboratory of Atomic and Subatomic Structure and Quantum Control (Ministry of Education),
Guangdong Basic Research Center of Excellence for Structure and Fundamental Interactions of Matter,
School of Physics, South China Normal University, Guangzhou 510006, China*

²*Guangdong Provincial Key Laboratory of Quantum Engineering and Quantum Materials,
Guangdong-Hong Kong Joint Laboratory of Quantum Matter,
South China Normal University, Guangzhou 510006, China*

³*Quantum Science Center of Guangdong-HongKong-Macao Greater Bay Area(Guangdong), Shenzhen, 518000, China*

⁴*School of Electronic Science and Engineering (School of Microelectronics),
South China Normal University, Foshan 528225, China*

(Dated: December 6, 2024)

Over the past decade, parity-time (PT) symmetry and anti-PT (APT) symmetry in various physical systems have been extensively studied, leading to significant experimental and theoretical advancements. However, physical systems that simultaneously exhibit both PT and APT symmetry have not yet been explored. In this study, we construct a phase-sensitive non-Hermitian wave mixing model that inherently possesses single-mode APT symmetry. By tuning the phase of the pump field, this model simultaneously exhibits two-mode quadrature-PT symmetry. Moreover, the APT phase transition is accompanied by the emergence of quantum entanglement from absence to presence. This remarkable quantum effect, quantum entanglement, which distinguishes itself from classical physics, is surprisingly linked to APT symmetry phase transition. Our work further explores the relationship between two-mode quantum entanglement and the phase of the pump field, offering deeper insight into the generation and evolution of entanglement in the corresponding nonlinear system. This provides a new perspective on quantum information processing.

Introduction.—Although any Hermitian operator has real eigenvalues, hermiticity is not a necessary condition to obtain real eigenvalues. Recent studies have shown that any Hamiltonian satisfying parity-time (PT) symmetry ($[H, PT] = 0$) can still possess real eigenvalues [1–3]. Such systems undergo a phase transition during which the PT symmetry is spontaneously broken. The eigenvalues of the Hamiltonian transition from real to complex at a specific point in the parameter space are known as the exceptional point (EP). At the EP, both the eigenvalues and eigenvectors of the Hamiltonian coalesce, leading to a range of novel phenomena [4–10]. Corresponding to PT symmetry, anti-PT (APT) symmetry, as another form of non-Hermitian symmetry ($\{H, PT\} = 0$), also undergoes spontaneous APT symmetry breaking during the APT phase transition, accompanied by the emergence of EPs [11, 12].

Over the past decade, PT symmetry [13–25] and APT symmetry [26–33] in various physical systems such as photonics, acoustics, and ultracold atoms have been extensively explored, leading to significant experimental and theoretical advancements. To realize PT symmetry in a physical system, the system typically exhibits linear gain and loss [3, 4, 26, 34]. However, these optical gain and loss mechanisms present significant challenges for achieving PT symmetry in the purely quantum realm [35] because the associated Langevin noise disrupts PT symmetry in quantum systems [36, 37]. Currently, there are two approaches to circumvent this issue: one is a passive scheme based on loss modulation, and the other is the Hamiltonian dilation method [37–42]. By contrast,

APT symmetry can be realized without gain and loss [29, 43–45]. Recent theoretical research indicates that APT symmetry can be realized in a two-mode bosonic system without involving linear gain and loss of classical fields. This suggests the potential for achieving quantum APT symmetry free from Langevin noise, which can be implemented in nonlinear wave-mixing processes [45].

Recent studies focusing on quantum entanglement [46, 47] have demonstrated the unique properties of PT symmetry and APT symmetry in both two-qubit systems [48] and linear optical systems [49]. However, physical systems that simultaneously exhibit both PT symmetry and APT symmetry have not yet been explored.

In this study, we construct a phase-sensitive non-Hermitian wave mixing model that not only possesses inherent single-mode APT symmetry but also achieves two-mode quadrature-PT symmetry by modulating the phase of the pump field. This aspect has not been explored in previous studies. Classical-nonclassical polarity (CNP) reveals the unique impact of APT symmetry on the nonclassical properties of a system. Specifically, significant changes in the single-mode squeezing dynamics and two-body Gaussian entanglement dynamics of the system are observed as it traverses EP. Furthermore, the results from the inseparability criterion provide deeper insights into the relationship between two-mode quadrature-entanglement and the phase of the pump field. They reveal the influence of single-mode APT symmetry and two-mode quadrature-PT symmetry on the entanglement. Specifically, when the phase of the pump field satisfies $\cos \phi = 0$, the system simul-

aneously exhibits single-mode APT symmetry and two-mode quadrature-PT symmetry. Under these conditions, the two-mode quadrature-entanglement undergoes sudden death in the two-mode quadrature-PT-broken region and EP, while exhibiting periodic revival characteristics in the two-mode quadrature-PT-symmetric region. Conversely, when the phase of the pump field meets the condition $\cos \phi = \pm 1$, the phase transition of the system from the APT-symmetric region to the APT-broken region is accompanied by the emergence of quantum entanglement from nonexistence (symbolizing a transition from classical to quantum). Our work further investigates the unique non-Hermitian properties of nonlinear systems, exploring the relationship between two-mode quantum entanglement and the phase of the pump field. This deeper examination reveals the entanglement generation and evolution process in the corresponding nonlinear system of the model, offering new perspectives for quantum information processing.

Theoretical model.—Consider the Four-wave mixing process shown in Fig. 1(a). The input pump field ω_p with phase φ and coherent state input signal field ω_s (idler field ω_i) are incident onto a nonlinear medium (where χ represents the nonlinear susceptibility of the medium). During this process, two pump photons are annihilated and one signal photon and one idler photon are simultaneously generated. Considering an undepleted pump field, in the classical parametric approximation, the coupling equations between the signal field operator a_s and idler field operator a_i can be written as (we set $\hbar = 1$) [12, 29]

$$i\partial_z(a_s, a_i^\dagger)^T = H_{\text{single-mode}}(a_s, a_i^\dagger)^T. \quad (1)$$

The non-Hermitian Hamiltonian matrix $H_{\text{single-mode}}$ in Eq. (1) is

$$H_{\text{single-mode}} = \begin{pmatrix} \Delta & \kappa e^{-i\phi} \\ -\kappa e^{i\phi} & -\Delta \end{pmatrix} \quad (2)$$

where $\phi = 2\varphi$, κ is the real nonlinear coupling coefficient, and $\Delta = -\Delta k/2$. As shown in Fig. 1(a), the phase mismatch $\Delta k = 2k_p - (k_s + k_i) \cos \theta$, where k_p , k_s , and k_i represent the wave numbers of the pump (ω_p), signal (ω_s), and idler fields (ω_i), respectively. Obviously, no matter the value of the phase ϕ , $H_{\text{single-mode}}$ satisfies $\{H_{\text{single-mode}}, PT\} = 0$, where P is the parity operator and T is the time-reversal operator. This indicates that the single-mode system exhibits APT symmetry. Since there is no involvement of loss in $H_{\text{single-mode}}$, the Langevin noise operator does not need to be considered here to preserve the commutation relations $[a_j(0), a_j^\dagger(0)] = [a_j(L), a_j^\dagger(L)] = 1(j = s, i)$. The eigenvalues of $H_{\text{single-mode}}$ are given by $\lambda_{\pm} = \pm\lambda = \pm i|\kappa|\sqrt{1 - \delta^2}$, where $\delta = |\Delta/\kappa|$. As shown in Fig. 1(b), when $\delta < 1$, the eigenvalues are a pair of purely imaginary complex conjugates and the system is in the APT-symmetric region. When $\delta > 1$, the eigenvalues are

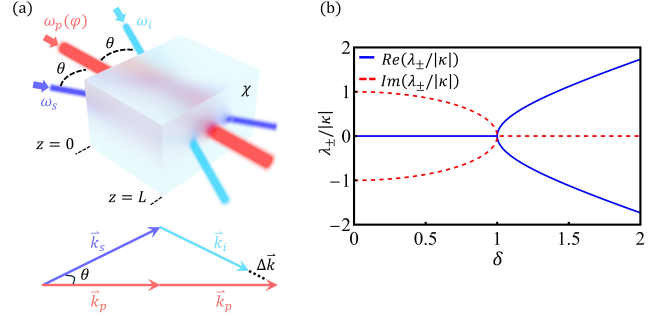


FIG. 1. (a) A non-Hermitian system composed of a four-wave mixing process and a phase-controllable pump source. χ represents the nonlinear susceptibility. φ is the phase of the pump field, θ is the angle between the pump field and the signal (idler) field, and L represents the total length of the nonlinear medium along the optical axis of the pump field. (b) APT phase transition process of the eigenvalues λ_{\pm} .

real and the system is in the APT-broken region. When $\delta = 1$, the system is at the EP, where $\lambda_0 = 0$, indicating spontaneous symmetry breaking in the system. Interestingly, by combining the quadrature of the optical field $q_j = \frac{1}{2}(a_j^\dagger + a_j)$ and $p_j = \frac{i}{2}(a_j^\dagger - a_j)$, where $[q_j, p_j] = \frac{i}{2}$, the dynamical equation between the two-mode quadrature can be rewritten as

$$i\partial_z(q_s + q_i, p_s + p_i)^T = H_{\text{two-mode}(+)}(q_s + q_i, p_s + p_i)^T, \quad (3a)$$

$$i\partial_z(p_s - p_i, q_s - q_i)^T = H_{\text{two-mode}(-)}(p_s - p_i, q_s - q_i)^T. \quad (3b)$$

In here, if and only if $\cos \phi = 0$, the corresponding effective Hamiltonians in Eqs. (3a) and (3b) are given by

$$H_{\text{two-mode}(+)} = \begin{pmatrix} -i\kappa \sin \phi & i\Delta \\ -i\Delta & i\kappa \sin \phi \end{pmatrix} \quad (4a)$$

$$H_{\text{two-mode}(-)} = \begin{pmatrix} -i\kappa \sin \phi & -i\Delta \\ i\Delta & i\kappa \sin \phi \end{pmatrix} \quad (4b)$$

which satisfying $[H_{\text{two-mode}(\pm)}, PT] = 0$, the two-mode effective Hamiltonian exhibits PT symmetry. The corresponding eigenvalues are given by $\lambda_{\text{two-mode}(\pm)} = \lambda_{\pm} = \pm|\kappa|\sqrt{\delta^2 - 1}$. When $\delta > 1$, the eigenvalues are real and the system is in the two-mode quadrature-PT-symmetric region. When $\delta < 1$, the eigenvalues are a pair of purely imaginary complex conjugates and the system is in the two-mode quadrature-PT-broken region. When $\delta = 1$, the system is at the EP, where $\lambda_0 = 0$, indicating spontaneous symmetry breaking. The solutions to Eqs. (1) and (3a)-(3b) can be found in the supplementary materials.

It is worth emphasizing that by satisfying a specific phase condition ($\cos \phi = 0$), this phase-sensitive non-Hermitian wave mixing model can simultaneously exhibit

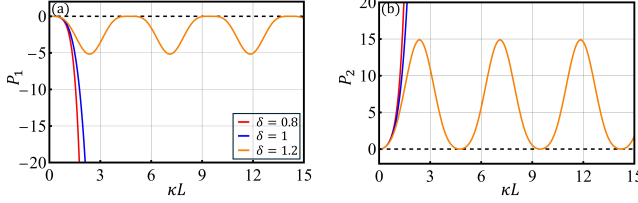


FIG. 2. CNP of the system. The evolution of P_1 (a) and P_2 (b). The red solid line (for $\delta = 0.8$) is in the APT-symmetric region, the blue solid line (for $\delta = 1$) is at the EP, and the orange solid line (for $\delta = 1.2$) is in the APT-broken region.

single-mode APT symmetry and two-mode quadrature-PT symmetry, which has not been explored in previous research.

Classical-Nonclassical Polarity.—To investigate the intrinsic connection between non-classical properties and the non-Hermitian nature of this phase-sensitive model, we first study Classical-Nonclassical Polarity (CNP) [50] in our model.

Using the covariance matrix γ_{si} (see supplementary materials for more detail), the single-mode and two-mode CNPs can be written as [50]

$$P_1 = -\frac{\kappa^4 \sin^4 \lambda L}{\lambda^4}, \quad (5a)$$

$$P_2 = -\frac{(\kappa^2 - 2\Delta^2 + \kappa^2 \cos 2\lambda L) \kappa^2 \sin^2 \lambda L}{\lambda^4}. \quad (5b)$$

P_1 characterizes the single-mode squeezing property of the system. In our model, the signal and idler fields exhibit the same single-mode squeezing properties. P_2 characterizes the two-mode Gaussian entanglement of the system. When the CNP is greater than 0, it indicates that the system is in a nonclassical state. When the CNP is equal to zero, the system is at the boundary between the classical and nonclassical states. When the CNP is less than 0, the system is in a classical state. The absolute value of the CNP quantifies the distance of the state from the classical-nonclassical boundary.

The nonclassical properties measured by CNP have two important characteristics. First, as shown in Eq. (5a) and (5b), the intensity of the input coherent state is independent of the nonclassical properties measured by the CNP. Second, the phase of the pump field is also independent of the nonclassical properties measured by the CNP, meaning that single-mode squeezing and two-mode Gaussian entanglement are not affected by the phase of the pump field. The nonclassical properties primarily depend on the system parameters κ and Δ , as well as the evolution distance κL . Therefore, discussing the CNP connection between single-mode APT symmetry and two-mode quadrature-PT symmetry here does not violate the condition $\cos \phi = 0$.

Fig. 2 (a) and (b) describe the evolution of P_1 and P_2 , respectively. In fig. 2(a), regardless of the single-

mode APT symmetry state, P_1 is less than or equal to 0, indicating that the system does not exhibit single-mode squeezing, and thus demonstrates classical characteristics. Correspondingly, regardless of how the two-mode quadrature-PT symmetry varies, P_2 is greater than or equal to 0 in fig. 2(b), indicating that the system consistently generates two-mode Gaussian entanglement throughout and reflecting nonclassical characteristics. More deeply, in single-mode APT-symmetric region and two-mode quadrature-PT-broken region ($\delta = 0.8$), one of the eigenmodes disappears after a long evolution length owing to the presence of purely imaginary eigenvalues λ_{\pm} . The two-mode Gaussian entanglement measured by P_2 shows a monotonic increase. In the single-mode APT-broken region and two-mode quadrature-PT-symmetric region ($\delta = 1.2$), the two-mode Gaussian entanglement exhibits oscillatory behavior with a period of $T = \kappa\pi/\lambda$. At the EP ($\delta = 1$), the two eigenmodes merge into a single mode. The two-mode Gaussian entanglement increases monotonically, but the rate of enhancement is slower compared to the single-mode APT-symmetric region and two-mode quadrature-PT-broken region. CNP reveals the unique connection between single-mode APT symmetry and two-mode quadrature-PT symmetry in the system's non-classical properties.

The inseparability criterion.—To further explore the system's nonclassical properties, we consider another characterization of quantum entanglement: the inseparability criterion [51, 52]. It reveals the relationship between system entanglement and the phase of the pump field and elucidates the impact of single-mode APT symmetry and two-mode quadrature-PT symmetry on entanglement.

The inseparability criterion is defined as follows: $E_1 = \text{Var}(q_s - q_i) + \text{Var}(p_s + p_i)$, $E_2 = \text{Var}(q_s + q_i) + \text{Var}(p_s - p_i)$. E_1 and E_2 are referred to as type-I and type-II entanglements of the system, respectively. $E_1 < 1$ or $E_2 < 1$ corresponds to the weaker criterion (wc). When $E_1 < 0.5$ or $E_2 < 0.5$, it corresponds to the stronger criterion (sc). The closer the values of E_1 and E_2 are to 0, the higher the degree of entanglement.

The theoretical calculation results are as follows:

$$E_1 = \cos^2 \lambda L + \frac{(\kappa^2 + \Delta^2 + G1) \sin^2 \lambda L + G2}{\lambda^2} \quad (6a)$$

$$E_2 = \cos^2 \lambda L + \frac{(\kappa^2 + \Delta^2 - G1) \sin^2 \lambda L - G2}{\lambda^2} \quad (6b)$$

Where $G1 = 2\kappa\Delta \cos \phi$ and $G2 = \kappa\lambda \sin 2\lambda z \sin \phi$. Consider the input field as coherent state. From Eqs. (6a) and (6b), it is evident that the degree of entanglement is independent of the intensity of the input field. Instead, it is determined by the system parameters κ and Δ and the evolution distance κL , and is also influenced by the phase of the pump field. Under different phase conditions (e.g., $\cos \phi = \pm 1$ or $\cos \phi = 0$), the system exhibits distinct entanglement evolution characteristics.

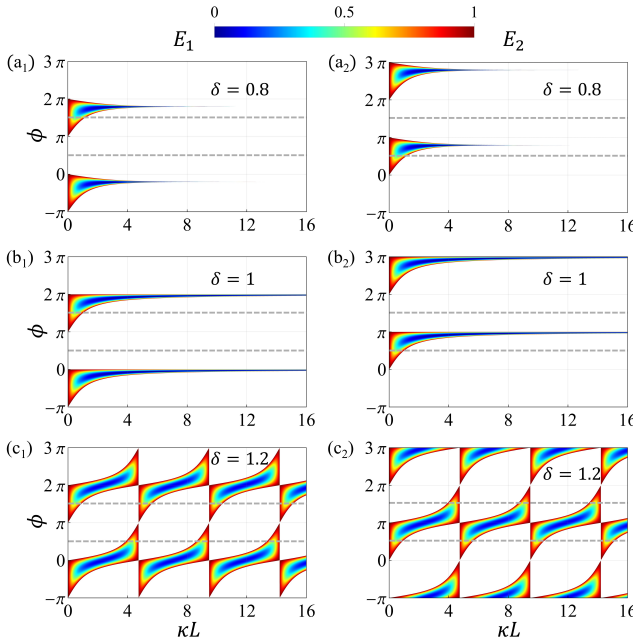


FIG. 3. The evolution of the type-I/type-II entanglement under different phase ϕ : (a₁), (b₁), and (c₁) correspond to type-I entanglement E_1 ; (a₂), (b₂), and (c₂) correspond to type-II entanglement E_2 . (a₁) and (a₂) show the system in the APT-symmetric region with $\delta = 0.8$; (b₁) and (b₂) show the system at the EP with $\delta = 1$; (c₁) and (c₂) show the system in the APT-broken region with $\delta = 1.2$. The dashed gray line indicates that the evolution simultaneously satisfies two-mode quadrature-PT symmetry($\cos \phi = 0$).

Fig.3 shows the evolution of type-I/type-II entanglement in different phase ϕ . When the phase ϕ satisfies $\cos \phi = 0$ (e.g., $\phi = 1.5\pi$ or 0.5π), the system simultaneously exhibits single-mode APT symmetry and two-mode quadrature-PT symmetry, as shown by the dashed gray line. By comparing fig.3 (a₁), (b₁), and (c₁) with fig.3 (a₂), (b₂), and (c₂), it can be seen that the type-I entanglement E_1 and type-II entanglement E_2 differ only by a phase of π . Therefore, the following analysis focuses on the type-I entanglement E_1 . Fig.3(a₁) shows that when the system is in the single-mode APT-symmetric region ($\delta = 0.8$) and the phase ϕ satisfies $\pi < \phi < 2\pi$, the system is still capable of generating entanglement. However, as the system evolves, entanglement is maintained within a very narrow phase range. Outside this range, entanglement briefly exists before rapidly vanishing. When the phase ϕ assumes other values (e.g., $0 < \phi < \pi$), no entanglement is generated in the system. Fig.3(c₁) shows that in the single-mode APT-broken region ($\delta = 1.2$), the evolution of the system entanglement exhibits an oscillatory pattern with a period $T = \kappa\pi/\lambda$. The degree of entanglement can be tuned by varying the phase ϕ . Interestingly, as shown in Fig.3(b₁), when the system is at the EP ($\delta = 1$), by tuning the phase ϕ close to 0, en-

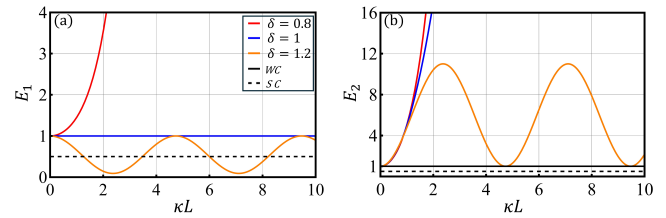


FIG. 4. The evolution of entanglement when the pump phase satisfies $\cos \phi = 1$. The solid red line represents the single-mode APT-symmetric region ($\delta = 0.8$), the solid blue line indicates the EP ($\delta = 1$), the solid orange line denotes the single-mode APT-broken region ($\delta = 1.2$), the solid black line represents the weaker criterion (wc) for entanglement, and the dashed black line corresponds to the stronger criterion (sc) for entanglement. (a) Evolution of type-I entanglement. (b) Evolution of type-II entanglement.

tanglement can be maintained over a wider phase range than in the single-mode APT-symmetric region. This demonstrates the significant role of EP control in non-Hermitian systems and phase ϕ tuning in the generation of entanglement in this model.

Specifically, when the system is at the EP ($\delta = 1$), the expressions for E_1 and E_2 are simplified to

$$E_1 = 1 + 2\kappa^2 L^2 - 2\kappa^2 L^2 \cos \phi + 2\kappa L \sin \phi \quad (7a)$$

$$E_2 = 1 + 2\kappa^2 L^2 + 2\kappa^2 L^2 \cos \phi - 2\kappa L \sin \phi \quad (7b)$$

It can be observed that when the phase condition $\cos \phi = 1$ (or $\cos \phi = -1$) is met, $E_1 = 1$ (or $E_2 = 1$) is independent of the propagation distance, indicating that the system is in a critical state between the classical and quantum regimes.

Fig. 4 clearly reveals the unique phenomenon that occurs in the system when the phase of the pump field satisfies the condition $\cos \phi = 1$. As shown in Fig. 4(a), for type-I entanglement E_1 , at the EP ($\delta = 1$), $E_1 = 1$ represents a critical state between the classical and quantum regimes. No entanglement was observed in the single-mode APT-symmetric region ($\delta = 0.8$). In the single-mode APT-broken region ($\delta = 1.2$), the system consistently exhibits and maintains a certain degree of entanglement, with the entanglement degree oscillating with a period $T = \kappa\pi/\lambda$. The phase transition of the system from the APT-symmetric region through the EP to the APT-broken region is accompanied by a transition of quantum entanglement from nonexistence to presence, symbolizing a shift from classical to quantum behavior. The remarkable quantum effect of quantum entanglement, which distinguishes it from classical physics, is linked to APT symmetry phase transition. For type-II entanglement as shown in fig. 4(b), no entanglement is generated under this phase setting.

Conclusion.—In summary, unlike previous studies, this study introduces a phase-sensitive non-Hermitian four-wave mixing model. The single-mode effective

Hamiltonian of this model satisfies APT symmetry, and by adjusting the phase of the pump field, the two-mode effective Hamiltonian can simultaneously exhibit two-mode quadrature-PT symmetry. By analyzing the system's non-classical characteristics through CNP and the inseparability criterion, it is found that the single-mode squeezing and two-mode Gaussian entanglement measured by CNP are independent of the phase of the pump field, whereas the two-mode quadrature-entanglement measured by the inseparability criterion is phase-dependent. This is primarily because CNP measures the overall non-classicality of the system, whereas the inseparability criterion assesses the entanglement between quadrature components of the two-mode fields. Consequently, they reveal different aspects of non-classical properties.

Theoretical calculations of the inseparability criterion show that, when the pump phase satisfies $\cos \phi = 0$, the system simultaneously exhibits single-mode APT symmetry and two-mode quadrature-PT symmetry. Under these conditions, quantum entanglement undergoes sudden death in the two-mode quadrature-PT-broken region and EP, whereas it exhibits periodic revival characteristics in the two-mode quadrature-PT-symmetric region. When the pump phase satisfies the condition $\cos \phi = \pm 1$, the phase transition of the system from the APT-symmetric region through the EP to the APT-broken region is accompanied by a transition of quantum entanglement from nonexistence to existence, symbolizing a shift from classical to quantum behavior. Our work further explores the unique non-Hermitian properties of nonlinear systems, investigates the relationship between two-mode quantum entanglement and the pump phase, and provides a deeper understanding of the entanglement generation and evolution processes in the model. This study offers new insights into quantum information processing.

Acknowledgments.—This work was supported by the Innovation Program for Quantum Science and Technology (Grant No.2021ZD0303401), the Quantum Science Strategic Project of Guangdong Province (Grant No.GDZX2306004), the National Natural Science Foundation of China under (No.Grant 62375089 and No.Grant 62471188), and Guangdong Basic and Applied Basic Research Foundation (Grant No.2022A1515140139).

- [3] R. El-Ganainy, K. G. Makris, M. Khajavikhan, Z. H. Musslimani, S. Rotter, and D. N. Christodoulides, Non-Hermitian physics and PT symmetry, *Nature Physics* **14**, 11 (2018).
- [4] S. K. Özdemir, S. Rotter, F. Nori, and L. Yang, Parity-time symmetry and exceptional points in photonics, *Nature Materials* **18**, 783 (2019).
- [5] E. J. Bergholtz, J. C. Budich, and F. K. Kunst, Exceptional topology of non-Hermitian systems, *Reviews of Modern Physics* **93**, 015005 (2021).
- [6] K. Ding, C. Fang, and G. Ma, Non-Hermitian topology and exceptional-point geometries, *Nature Reviews Physics* **4**, 745 (2022).
- [7] C. Wang, Z. Fu, W. Mao, J. Qie, A. D. Stone, and L. Yang, Non-Hermitian optics and photonics: From classical to quantum, *Advances in Optics and Photonics* **15**, 442 (2023).
- [8] W. Chen, S. Kaya Özdemir, G. Zhao, J. Wiersig, and L. Yang, Exceptional points enhance sensing in an optical microcavity, *Nature* **548**, 192 (2017).
- [9] W.-C. Wang, Y.-L. Zhou, H.-L. Zhang, J. Zhang, M.-C. Zhang, Y. Xie, C.-W. Wu, T. Chen, B.-Q. Ou, W. Wu, H. Jing, and P.-X. Chen, Observation of PT-symmetric quantum coherence in a single-ion system, *Physical Review A* **103**, L020201 (2021).
- [10] P.-R. Han, F. Wu, X.-J. Huang, H.-Z. Wu, C.-L. Zou, W. Yi, M. Zhang, H. Li, K. Xu, D. Zheng, H. Fan, J. Wen, Z.-B. Yang, and S.-B. Zheng, Exceptional Entanglement Phenomena: Non-Hermiticity Meeting Non-classicality, *Physical Review Letters* **131**, 260201 (2023).
- [11] L. Ge and H. E. Türeci, Antisymmetric PT-photonics structures with balanced positive- and negative-index materials, *Physical Review A* **88**, 053810 (2013).
- [12] Z. Niu, Y. Jiang, J. Wen, C. Zhang, S. Du, and I. Novikova, Four-wave mixing with anti-parity-time symmetry in hot 85Rb vapor, *Applied Physics Letters* **124**, 044005 (2024).
- [13] R. El-Ganainy, K. G. Makris, D. N. Christodoulides, and Z. H. Musslimani, Theory of coupled optical PT-symmetric structures, *Optics Letters* **32**, 2632 (2007).
- [14] A. Guo, G. J. Salamo, D. Duchesne, R. Morandotti, M. Volatier-Ravat, V. Aimez, G. A. Siviloglou, and D. N. Christodoulides, Observation of PT-Symmetry Breaking in Complex Optical Potentials, *Physical Review Letters* **103**, 093902 (2009).
- [15] C. E. Rüter, K. G. Makris, R. El-Ganainy, D. N. Christodoulides, M. Segev, and D. Kip, Observation of parity-time symmetry in optics, *Nature Physics* **6**, 192 (2010).
- [16] J. Schindler, A. Li, M. C. Zheng, F. M. Ellis, and T. Kottos, Experimental study of active LRC circuits with PT symmetries, *Physical Review A* **84**, 040101 (2011).
- [17] C. Hang, G. Huang, and V. V. Konotop, PT Symmetry with a System of Three-Level Atoms, *Physical Review Letters* **110**, 083604 (2013).
- [18] B. Peng, S. K. Özdemir, F. Lei, F. Monifi, M. Gianfreda, G. L. Long, S. Fan, F. Nori, C. M. Bender, and L. Yang, Parity-time-symmetric whispering-gallery microcavities, *Nature Physics* **10**, 394 (2014).
- [19] J. Wiersig, Enhancing the Sensitivity of Frequency and Energy Splitting Detection by Using Exceptional Points: Application to Microcavity Sensors for Single-Particle Detection, *Physical Review Letters* **112**, 203901 (2014).

* These authors contributed equally to this work.

† dmliu@scnu.edu.cn

‡ mingu@m.scnu.edu.cn

- [1] C. M. Bender and S. Boettcher, Real Spectra in Non-Hermitian Hamiltonians Having PT Symmetry, *Physical Review Letters* **80**, 5243 (1998).
- [2] C. M. Bender, Making sense of non-Hermitian Hamiltonians, *Reports on Progress in Physics* **70**, 947 (2007).

[20] X. Zhu, H. Ramezani, C. Shi, J. Zhu, and X. Zhang, PT-Symmetric Acoustics, *Physical Review X* **4**, 031042 (2014).

[21] L. Feng, Z. J. Wong, R.-M. Ma, Y. Wang, and X. Zhang, Single-mode laser by parity-time symmetry breaking, *Science* **346**, 972 (2014).

[22] H. Hodaei, M.-A. Miri, M. Heinrich, D. N. Christodoulides, and M. Khajavikhan, Parity-time-symmetric microring lasers, *Science* [10.1126/science.1258480](https://doi.org/10.1126/science.1258480) (2014).

[23] R. Fleury, D. Sounas, and A. Alù, An invisible acoustic sensor based on parity-time symmetry, *Nature Communications* **6**, 5905 (2015).

[24] Z.-P. Liu, J. Zhang, S. K. Özdemir, B. Peng, H. Jing, X.-Y. Lü, C.-W. Li, L. Yang, F. Nori, and Y.-x. Liu, Metrology with PT-Symmetric Cavities: Enhanced Sensitivity near the PT-Phase Transition, *Physical Review Letters* **117**, 110802 (2016).

[25] Z. Zhang, Y. Zhang, J. Sheng, L. Yang, M.-A. Miri, D. N. Christodoulides, B. He, Y. Zhang, and M. Xiao, Observation of Parity-Time Symmetry in Optically Induced Atomic Lattices, *Physical Review Letters* **117**, 123601 (2016).

[26] P. Peng, W. Cao, C. Shen, W. Qu, J. Wen, L. Jiang, and Y. Xiao, Anti-parity-time symmetry with flying atoms, *Nature Physics* **12**, 1139 (2016).

[27] Y. Li, Y.-G. Peng, L. Han, M.-A. Miri, W. Li, M. Xiao, X.-F. Zhu, J. Zhao, A. Alù, S. Fan, and C.-W. Qiu, Anti-parity-time symmetry in diffusive systems, *Science* **364**, 170 (2019).

[28] X.-L. Zhang, T. Jiang, and C. T. Chan, Dynamically encircling an exceptional point in anti-parity-time symmetric systems: Asymmetric mode switching for symmetry-broken modes, *Light: Science & Applications* **8**, 88 (2019).

[29] Y. Jiang, Y. Mei, Y. Zuo, Y. Zhai, J. Li, J. Wen, and S. Du, Anti-Parity-Time Symmetric Optical Four-Wave Mixing in Cold Atoms, *Physical Review Letters* **123**, 193604 (2019).

[30] W. Cao, X. Lu, X. Meng, J. Sun, H. Shen, and Y. Xiao, Reservoir-Mediated Quantum Correlations in Non-Hermitian Optical System, *Physical Review Letters* **124**, 030401 (2020).

[31] H. Fan, J. Chen, Z. Zhao, J. Wen, and Y.-P. Huang, Anti-parity-Time Symmetry in Passive Nanophotonics, *ACS Photonics* **7**, 3035 (2020).

[32] A. Bergman, R. Duggan, K. Sharma, M. Tur, A. Zadok, and A. Alù, Observation of anti-parity-time-symmetry, phase transitions and exceptional points in an optical fibre, *Nature Communications* **12**, 486 (2021).

[33] Z. Feng and X. Sun, Harnessing Dynamical Encircling of an Exceptional Point in Anti-PT-Symmetric Integrated Photonic Systems, *Physical Review Letters* **129**, 273601 (2022).

[34] D. Christodoulides and J. Yang, eds., *Parity-Time Symmetry and Its Applications*, Springer Tracts in Modern Physics, Vol. 280 (Springer, Singapore, 2018).

[35] S. Scheel and A. Szameit, PT-symmetric photonic quantum systems with gain and loss do not exist, *Europhysics Letters* **122**, 34001 (2018).

[36] M. Zhang, W. Sweeney, C. W. Hsu, L. Yang, A. D. Stone, and L. Jiang, Quantum Noise Theory of Exceptional Point Amplifying Sensors, *Physical Review Letters* **123**, 180501 (2019).

[37] M. Naghiloo, M. Abbasi, Y. N. Joglekar, and K. W. Murch, Quantum state tomography across the exceptional point in a single dissipative qubit, *Nature Physics* **15**, 1232 (2019).

[38] Y. Wu, W. Liu, J. Geng, X. Song, X. Ye, C.-K. Duan, X. Rong, and J. Du, Observation of parity-time symmetry breaking in a single-spin system, *Science* **364**, 878 (2019).

[39] F. Klauck, L. Teuber, M. Ornigotti, M. Heinrich, S. Scheel, and A. Szameit, Observation of PT-symmetric quantum interference, *Nature Photonics* **13**, 883 (2019).

[40] S. Yu, Y. Meng, J.-S. Tang, X.-Y. Xu, Y.-T. Wang, P. Yin, Z.-J. Ke, W. Liu, Z.-P. Li, Y.-Z. Yang, G. Chen, Y.-J. Han, C.-F. Li, and G.-C. Guo, Experimental Investigation of Quantum PT-Enhanced Sensor, *Physical Review Letters* **125**, 240506 (2020).

[41] L. Ding, K. Shi, Q. Zhang, D. Shen, X. Zhang, and W. Zhang, Experimental Determination of PT-Symmetric Exceptional Points in a Single Trapped Ion, *Physical Review Letters* **126**, 083604 (2021).

[42] W. Liu, Y. Wu, C.-K. Duan, X. Rong, and J. Du, Dynamically Encircling an Exceptional Point in a Real Quantum System, *Physical Review Letters* **126**, 170506 (2021).

[43] M.-A. Miri and A. Alù, Nonlinearity-induced PT-symmetry without material gain, *New Journal of Physics* **18**, 065001 (2016).

[44] Y.-X. Wang and A. A. Clerk, Non-Hermitian dynamics without dissipation in quantum systems, *Physical Review A* **99**, 063834 (2019).

[45] X.-W. Luo, C. Zhang, and S. Du, Quantum Squeezing and Sensing with Pseudo-Anti-Parity-Time Symmetry, *Physical Review Letters* **128**, 173602 (2022).

[46] A. Einstein, B. Podolsky, and N. Rosen, Can Quantum-Mechanical Description of Physical Reality Be Considered Complete?, *Physical Review* **47**, 777 (1935).

[47] M. D. Reid, P. D. Drummond, W. P. Bowen, E. G. Cavalcanti, P. K. Lam, H. A. Bachor, U. L. Andersen, and G. Leuchs, Colloquium: The Einstein-Podolsky-Rosen paradox: From concepts to applications, *Reviews of Modern Physics* **81**, 1727 (2009).

[48] J. Zhang, Y.-L. Zhou, Y. Zuo, H. Zhang, P.-X. Chen, H. Jing, and L.-M. Kuang, Exceptional Entanglement and Quantum Sensing with a Parity-Time-Symmetric Two-Qubit System, *Advanced Quantum Technologies* **7**, 2300350 (2024).

[49] Y.-L. Fang, J.-L. Zhao, D.-X. Chen, Y.-H. Zhou, Y. Zhang, Q.-C. Wu, C.-P. Yang, and F. Nori, Entanglement dynamics in anti-PT-symmetric systems, *Physical Review Research* **4**, 033022 (2022).

[50] J. Liu, W. Ge, and M. S. Zubairy, Classical-Nonclassical Polarity of Gaussian States, *Physical Review Letters* **132**, 240201 (2024).

[51] L.-M. Duan, G. Giedke, J. I. Cirac, and P. Zoller, Inseparability Criterion for Continuous Variable Systems, *Physical Review Letters* **84**, 2722 (2000).

[52] R. Simon, Peres-Horodecki Separability Criterion for Continuous Variable Systems, *Physical Review Letters* **84**, 2726 (2000).

Supplementary Materials for "Squeezing and Entanglement Dynamics in Phase-Sensitive Non-Hermitian Systems"

Ruicong Huang,^{1,2,3,*} Wencong Wang,^{3,4,*} Yuyang

Liang,^{1,2,3} Dongmei Liu,^{3,4,†} and Min Gu^{1,2,3,‡}

¹*Key Laboratory of Atomic and Subatomic Structure*

and Quantum Control (Ministry of Education),

Guangdong Basic Research Center of Excellence for Structure

and Fundamental Interactions of Matter, School of Physics,

South China Normal University, Guangzhou 510006, China

²*Guangdong Provincial Key Laboratory of Quantum Engineering and Quantum Materials,*

Guangdong-Hong Kong Joint Laboratory of Quantum Matter,

South China Normal University, Guangzhou 510006, China

³*Quantum Science Center of Guangdong-HongKong-Macao*

Greater Bay Area(Guangdong), Shenzhen, 518000, China

⁴*School of Electronic Science and Engineering (School of Microelectronics),*

South China Normal University, Foshan 528225, China

S1.SUPPLEMENTARY MATERIAL ON DYNAMICAL EQUATION

The solution to dynamical equation (1) can be expressed in the following matrix form:

$$\begin{pmatrix} a_s(L) \\ a_i^\dagger(L) \end{pmatrix} = \begin{pmatrix} \cos \lambda L - i \frac{\Delta}{\lambda} \sin \lambda L & -ie^{-i\phi} \frac{\kappa}{\lambda} \sin \lambda L \\ ie^{i\phi} \frac{\kappa}{\lambda} \sin \lambda L & \cos \lambda L + i \frac{\Delta}{\lambda} \sin \lambda L \end{pmatrix} \begin{pmatrix} a_s(0) \\ a_i^\dagger(0) \end{pmatrix} \quad (\text{S1})$$

Throughout the dynamic process, it is straightforward to obtain $[a_j(L), a_j^\dagger(L)] = [a_j(0), a_j^\dagger(0)] = 1$ ($j = s, i$). The commutation relations of the modes are consistently preserved.

By combining the quadrature of the optical field $q_j = \frac{1}{2} (a_j + a_j^\dagger)$ and $p_j = -\frac{i}{2} (a_j - a_j^\dagger)$, where $j = s, i$, and $[q_j, p_j] = \frac{i}{2}$. Equation (1) can be transformed into

$$i\partial_z \begin{pmatrix} q_s + q_i \\ p_s + p_i \end{pmatrix} = i \begin{pmatrix} -\kappa \sin \phi & \Delta - \kappa \cos \phi \\ -\Delta - \kappa \cos \phi & \kappa \sin \phi \end{pmatrix} \begin{pmatrix} q_s + q_i \\ p_s + p_i \end{pmatrix} \quad (\text{S2a})$$

$$i\partial_z \begin{pmatrix} p_s - p_i \\ q_s - q_i \end{pmatrix} = i \begin{pmatrix} -\kappa \sin \phi & -\Delta + \kappa \cos \phi \\ \Delta + \kappa \cos \phi & \kappa \sin \phi \end{pmatrix} \begin{pmatrix} p_s - p_i \\ q_s - q_i \end{pmatrix} \quad (\text{S2b})$$

The solutions to dynamical equations (S2a) and (S2b) can be expressed in the following matrix form:

$$\begin{pmatrix} q_s(L) + q_i(L) \\ p_s(L) + p_i(L) \end{pmatrix} = \begin{pmatrix} \cos \lambda L - \frac{\kappa}{\lambda} \sin \lambda L \sin \phi & \frac{\Delta}{\lambda} \sin \lambda L - \frac{\kappa}{\lambda} \sin \lambda L \cos \phi \\ -\frac{\Delta}{\lambda} \sin \lambda L - \frac{\kappa}{\lambda} \sin \lambda L \cos \phi & \cos \lambda L + \frac{\kappa}{\lambda} \sin \lambda L \sin \phi \end{pmatrix} \begin{pmatrix} q_s(0) + q_i(0) \\ p_s(0) + p_i(0) \end{pmatrix} \quad (\text{S3a})$$

$$\begin{pmatrix} p_s(L) - p_i(L) \\ q_s(L) - q_i(L) \end{pmatrix} = \begin{pmatrix} \cos \lambda L - \frac{\kappa}{\lambda} \sin \lambda L \sin \phi & -\frac{\Delta}{\lambda} \sin \lambda L + \frac{\kappa}{\lambda} \sin \lambda L \cos \phi \\ \frac{\Delta}{\lambda} \sin \lambda L + \frac{\kappa}{\lambda} \sin \lambda L \cos \phi & \cos \lambda L + \frac{\kappa}{\lambda} \sin \lambda L \sin \phi \end{pmatrix} \begin{pmatrix} p_s(0) - p_i(0) \\ q_s(0) - q_i(0) \end{pmatrix} \quad (\text{S3b})$$

S2.SINGLE-MODE QUADRATURE-VARIANCE AND LOGARITHMIC NEGATIVITY

To verify the single-mode CNP, we calculated the single-mode variances, $\text{Var}(q_s)$, $\text{Var}(p_s)$, $\text{Var}(q_i)$, and $\text{Var}(p_i)$. The variance is defined as $\text{Var}(X) = \langle X^2 \rangle - \langle X \rangle^2$.

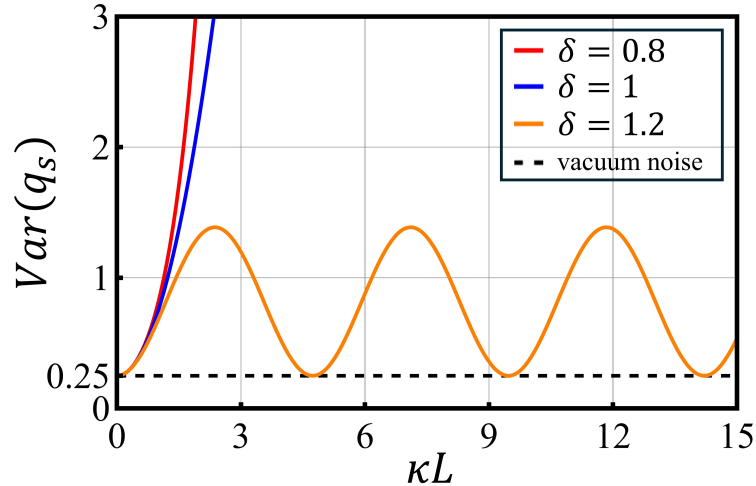


FIG. S1. Evolution of single-mode quadrature-variance $Var(q_s)$ for different values of δ . The solid red line ($\delta = 0.8$) represents the APT-symmetric region, solid blue line ($\delta = 1$) represents the EP, and solid orange line ($\delta = 1.2$) represents the APT-broken region. The dashed black line represents the vacuum noise level.

It is straightforward to obtain

$$Var(p_s) = Var(q_i) = Var(p_i) = Var(q_s) = \frac{\Delta^2 - \kappa^2 \cos(2L\sqrt{\Delta^2 - \kappa^2})}{4(\Delta^2 - \kappa^2)} \quad (S4)$$

Equation (S4) shows that the single-mode quadrature variances are independent of the input field intensity and the phase of the pump field.

Figure S1 shows the evolution of $Var(q_s)$. $Var(q_s)$ is greater than the vacuum noise in the APT-symmetric region, EP, and APT-broken region, indicating that the system does not exhibit single-mode squeezing and thus reflects classical characteristics. This corroborates the results of single-mode CNP discussed in the main text.

To verify the two-mode CNP, we calculate logarithmic negativity [1, 2] as an entanglement measure. This calculation requires the following covariance matrix of the system:

$$V = \begin{pmatrix} A & C \\ C^T & B \end{pmatrix} \quad (S5)$$

Where,

$$V_{nm} = \frac{1}{2} \langle X_n X_m + X_m X_n \rangle - \langle X_n \rangle \langle X_m \rangle \quad (S6)$$

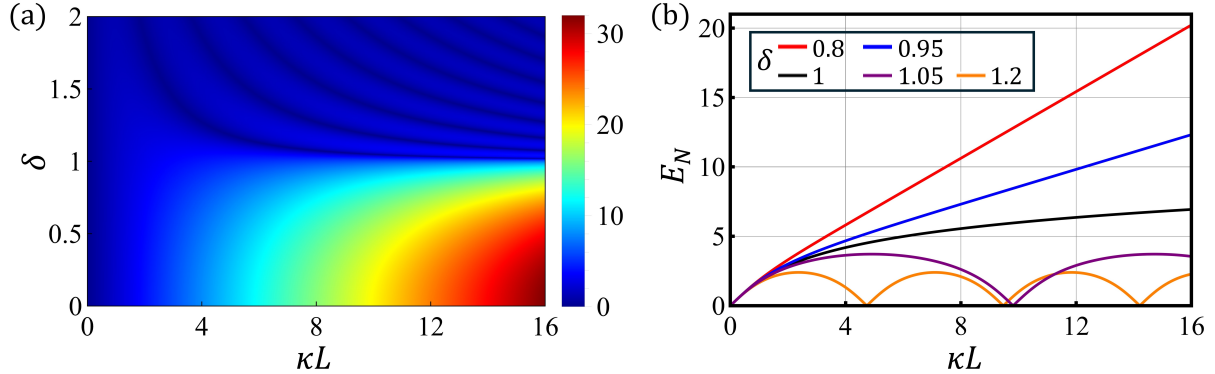


FIG. S2. Logarithmic negativity for the system (a) Variation of E_N with evolution distance κL and system parameter δ . (b) Evolution of E_N for different δ values. The red solid line ($\delta = 0.8$) and the blue solid line ($\delta = 0.95$) correspond to the APT-symmetric region, the black solid line ($\delta = 1$) corresponds to the EP, and the purple solid line ($\delta = 1.05$) and the orange solid line ($\delta = 1.2$) correspond to the APT-broken region.

Define $X(z) = [q_s(z), p_s(z), q_i(z), p_i(z)]^T$. The input signal and idler fields are initially in coherent states. The quantum states evolving according to the dynamical equations remain in Gaussian states, and all properties of these Gaussian states are encapsulated in the covariance matrix V . The logarithmic negativity can be calculated using the covariance matrix V as follows: $E_N = \max[0, -\ln 4\eta]$, where $\eta = \frac{1}{\sqrt{2}}\sqrt{\Sigma - \sqrt{\Sigma^2 - 4 \det V}}$ and $\Sigma = \det A + \det B - 2 \det C$. $E_N > 0$ indicates entanglement, with larger values of E_N corresponding to stronger entanglement.

The entanglement measured by logarithmic negativity has two important properties. First, as indicated by Equation (S6), the first and second terms on the right-hand side of the equation depend on the field operators. The difference between these terms ensures that the matrix elements of covariance matrix V are independent of the intensity of the input fields. Second, the entanglement measured by logarithmic negativity is also independent of the pump phase. The degree of entanglement primarily depends on the system parameters κ and Δ , as well as the evolution distance κL .

Figure S2(a) shows the entanglement results (measured by the logarithmic negativity E_N) as a function of the system parameter δ and the evolution distance κL . It is evident that significant changes in the entanglement behavior occur near the EP ($\delta = 1$). To illustrate the entanglement evolution more clearly, Figure S2(b) shows the entanglement dynamics for

$\delta = 0.8, 0.95, 1, 1.05$, and 1.2 . The results indicate that entanglement exhibits different evolution patterns in the APT-symmetric region, EP, and APT-broken region. In the APT-symmetric region ($\delta < 1$), owing to the presence of pure imaginary eigenvalues λ_{\pm} , one of the eigenmodes disappears after prolonged evolution, resulting in a monotonic increase in the entanglement of the system. Moreover, as the value of δ decreases (where $\delta = |\Delta/\kappa|$), assuming that κ is fixed and Δ decreases), the rate of entanglement enhancement in the system also increases. When $\delta \rightarrow 0$ ($\Delta \rightarrow 0$), the rate of entanglement enhancement reaches its maximum, which corresponds to a perfect phase-matching condition in the nonlinear process. In the APT-broken region ($\delta > 1$), the entanglement exhibits an oscillatory behavior with a period $T = \kappa\pi/\lambda$. The closer δ is to the EP, the longer the oscillation period and the stronger the achievable entanglement. At the EP ($\delta = 1$), the two eigenmodes merge into a single mode, leading to a monotonic increase in entanglement, although the rate of enhancement is slower than that in the APT-symmetric region. In summary, the entanglement measured by logarithmic negativity corroborates the results obtained from the two-mode CNP discussed in the main text.

S3.A SIMPLE VERIFICATION OF COMMUTATION RELATIONS

Through algebraic manipulations, it can be verified that the solutions provided in Equation (S1) consistently maintain the commutation relations

$$[a_s(L), a_s^\dagger(L)] = \left(\cos^2 \lambda L + \frac{\Delta^2 \sin^2 \lambda L}{\lambda^2} \right) [a_s(0), a_s^\dagger(0)] - \frac{\kappa^2 \sin^2 \lambda L}{\lambda^2} [a_i(0), a_i^\dagger(0)] = 1 \quad (\text{S7})$$

S4.CALCULATION OF CNP

To calculate CNP[3], a system covariance matrix is required. The covariance matrix of the system can be expressed as

$$\gamma_{si} = \begin{pmatrix} \gamma_s & x \\ x^\dagger & \gamma_i \end{pmatrix} \quad (\text{S8})$$

Where,

$$\gamma_{nm} = \frac{1}{2} \langle \Delta r_n \Delta r_m^\dagger + \Delta r_m^\dagger \Delta r_n \rangle \quad (\text{S9})$$

Define $r = [a_s^\dagger, a_s, a_i^\dagger, a_i]^\dagger$ and $\Delta r_n = r_n - \langle r \rangle_n$. The initial states of both the input signal field and idler field under study are in the coherent state. According to the dynamical equations, the evolving quantum state remains in a Gaussian state, and all properties of this Gaussian state are encapsulated in the covariance matrix γ_{si} .

$$\gamma_{si} = \begin{pmatrix} \frac{\Delta^2 - \kappa^2 \cos 2\lambda L}{2(\Delta^2 - \kappa^2)} & 0 & 0 & -\frac{e^{-i\phi}\kappa(\Delta + i\lambda \cot \lambda L) \sin^2 \lambda L}{\Delta^2 - \kappa^2} \\ 0 & \frac{\Delta^2 - \kappa^2 \cos 2\lambda L}{2(\Delta^2 - \kappa^2)} & \frac{e^{i\phi}\kappa(-\Delta + i\lambda \cot \lambda L) \sin^2 \lambda L}{\Delta^2 - \kappa^2} & 0 \\ 0 & \frac{e^{-i\phi}\kappa(-\Delta - i\lambda \cot \lambda L) \sin^2 \lambda L}{\Delta^2 - \kappa^2} & \frac{\Delta^2 - \kappa^2 \cos 2\lambda L}{2(\Delta^2 - \kappa^2)} & 0 \\ -\frac{e^{i\phi}\kappa(\Delta - i\lambda \cot \lambda L) \sin^2 \lambda L}{\Delta^2 - \kappa^2} & 0 & 0 & \frac{\Delta^2 - \kappa^2 \cos 2\lambda L}{2(\Delta^2 - \kappa^2)} \end{pmatrix} \quad (S10)$$

Using the covariance matrix γ_{si} , the single-mode and two-mode CNPs can be written as

$$P_1 = -\left(v - \frac{1}{2}\right)\left(N - \frac{1}{2}\right) = -\frac{\kappa^4 \sin^4 \lambda L}{\lambda^4} \quad (S11)$$

$$P_2 = -\frac{1}{8} + \frac{1}{2}I_1 - 2I_0 = -\frac{(\kappa^2 - 2\Delta^2 + \kappa^2 \cos 2\lambda L) \kappa^2 \sin^2 \lambda L}{\lambda^4} \quad (S12)$$

Let ν and N be the eigenvalues of the matrices γ_s and γ_i , respectively. The single- and two-mode CNPs are then given by $I_1 = |\gamma_s| + |\gamma_i| - 2|x|$, $I_0 = |\gamma_{si}|$.

S5. CALCULATION OF THE SEPARABILITY CRITERION

Through some straightforward algebraic manipulations, we obtain

$$Var(q_s - q_i) = Var(p_s + p_i) = \frac{(\Delta + \kappa \cos \phi)^2 \sin^2 \lambda L + (\lambda \cos \lambda L + \kappa \sin \lambda L \sin \phi)^2}{2\lambda^2} \quad (S13a)$$

$$Var(q_s + q_i) = Var(p_s - p_i) = \frac{(\Delta - \kappa \cos \phi)^2 \sin^2 \lambda L + (\lambda \cos \lambda L - \kappa \sin \lambda L \sin \phi)^2}{2\lambda^2} \quad (S13b)$$

By combining the definitions of the inseparability criteria, $E_1 = Var(q_s - q_i) + Var(p_s + p_i)$ and $E_2 = Var(q_s + q_i) + Var(p_s - p_i)$, the results for Equations (6a) and (6b) in the main text can be derived.

* These authors contributed equally to this work.

† dmliu@scnu.edu.cn

‡ mingu@m.scnu.edu.cn

- [1] G. Vidal and R. F. Werner, Computable measure of entanglement, *Physical Review A* **65**, 032314 (2002).
- [2] M. B. Plenio, Logarithmic Negativity: A Full Entanglement Monotone That is not Convex, *Physical Review Letters* **95**, 090503 (2005).
- [3] J. Liu, W. Ge, and M. S. Zubairy, Classical-Nonclassical Polarity of Gaussian States, *Physical Review Letters* **132**, 240201 (2024).